

PCCP

Accepted Manuscript



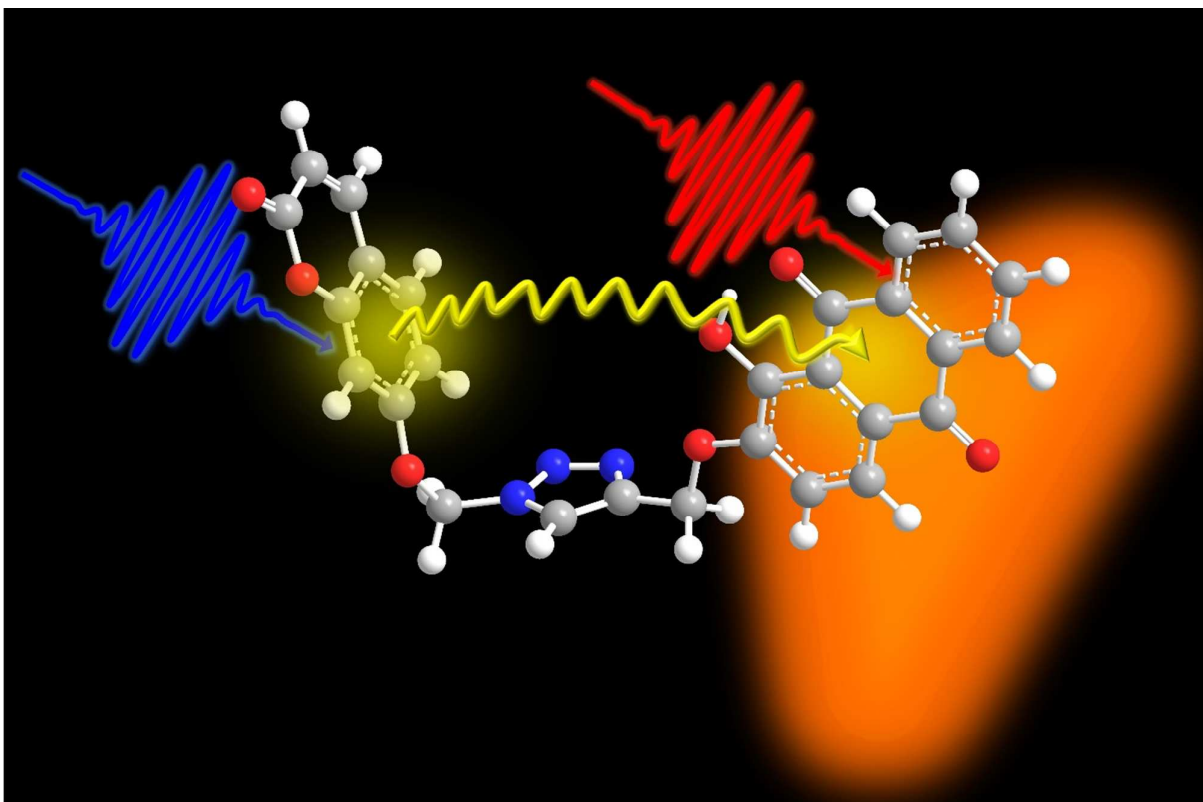
This is an *Accepted Manuscript*, which has been through the Royal Society of Chemistry peer review process and has been accepted for publication.

Accepted Manuscripts are published online shortly after acceptance, before technical editing, formatting and proof reading. Using this free service, authors can make their results available to the community, in citable form, before we publish the edited article. We will replace this *Accepted Manuscript* with the edited and formatted *Advance Article* as soon as it is available.

You can find more information about *Accepted Manuscripts* in the [Information for Authors](#).

Please note that technical editing may introduce minor changes to the text and/or graphics, which may alter content. The journal's standard [Terms & Conditions](#) and the [Ethical guidelines](#) still apply. In no event shall the Royal Society of Chemistry be held responsible for any errors or omissions in this *Accepted Manuscript* or any consequences arising from the use of any information it contains.

Fast and efficient intramolecular energy transfer takes place in Umbelliferone-Alizarin bichromophore; the process is well described the Förster mechanism



Ultrafast Resonance Energy Transfer in Umbelliferone-Alizarin Bichromophore

Andrea Lapini^{1,2,3}, Pierangelo Fabbrizzi³, Matteo Piccardo^{4,5}, Mariangela di Donato^{1,2,3}, Luisa Lascialfari³, Paolo Foggi^{1,2,6}, Stefano Cicchi³, Malgorzata Biczysko^{3,4}, Fabrizio Santoro⁷, Chiara Cappelli^{4,5} and Roberto Righini^{1,2,3}.

¹LENS (European laboratory for non linear spectroscopy) via N. Carrara 1, 50019 Sesto Fiorentino (FI) Italy

²INO (Istituto Nazionale di Ottica), Largo Fermi 6, 50125 Firenze, Italy

³Dipartimento di Chimica 'Ugo Schiff', Università di Firenze, via della Lastruccia 13, 50019 Sesto Fiorentino (FI), Italy

⁴Dipartimento di Chimica e Chimica Industriale, Università di Pisa, via Risorgimento 35, I-56126 Pisa Italy

⁵Scuola Normale Superiore, Piazza dei Cavalieri 7, I-56126 Pisa Italy

⁶Dipartimento di Chimica Università degli Studi di Perugia, via Elce di Sotto 8, 06123 Perugia, Italy

⁷CNR-Consiglio Nazionale delle Ricerche, Istituto di Chimica dei Composti Organo Metallici (ICCOM-CNR), UOS di Pisa, Area della Ricerca, via G. Moruzzi 1, I-56124 Pisa, Italy

Abstract

In this work we present the synthesis, time-resolved spectroscopic characterization and computational analysis of a bichromophore composed by two very well-known naturally occurring dyes: 7-hydroxycoumarin (Umbelliferone) and 1,2-dihydroxyanthraquinone (Alizarin). The Umbelliferone donor (**Dn**) and Alizarin acceptor (**Ac**) moieties are linked to a triazole ring *via* σ bonds, providing a flexible structure. By measuring the fluorescence quantum yields and the ultrafast transient absorption spectra we demonstrate the high efficiency ($\sim 85\%$) and the fast nature (~ 1.5 ps) of the energy transfer in this compound. Quantum chemical calculations, within the Density Functional Theory (DFT) approach, are used to characterize the electronic structure of the bichromophore (**Bi**) in the ground and excited state. We simulate the absorption and fluorescence spectra using the TD-DFT methods and the vertical gradient approach (VG), and include the solvent effects by adopting the Conductor-like Polarizable Continuum Model (CPCM). The calculated electronic structure suggests the occurrence of weak interactions between the electron densities of **Dn** and **Ac** in the excited state, indicating that the Förster-type transfer is the proper model for describing the energy transfer in this system. The averaged distance between **Dn** and **Ac** moieties calculated from the conformational analysis (12 Å) is in very good agreement with the value estimated from the Förster equation (~ 11 Å). At the same time, the calculated rate constant for energy transfer, averaged over multiple conformations of the system (3.6 ps), is in reasonable agreement with the experimental value (1.5 ps) estimated by transient absorption spectroscopy. The agreement between experimental results and

computational data lead us to conclude that the energy transfer in *Bi* is well described by the Förster mechanism.

Introduction

The process of electronic energy transfer (*EET*) is ubiquitous in natural and artificial photochemically active systems,¹ being of fundamental importance in the functioning of the antenna proteins of photosynthetic organisms² in multi-chromophoric systems,^{3, 4} in photo-molecular devices^{5, 6} and in photodynamic therapy⁷. In photosynthesis, for example, a complex pigment-protein system (the light-harvesting antenna) absorbs the solar photons and efficiently transfers the excitation energy to a reaction centre where it is converted into a trans-membrane electrochemical potential.^{8, 9} *EET* processes occur at distances ranging from 1 Å to more than 50 Å,⁹ and on time scales from femtoseconds to milliseconds. Understanding the geometrical and electronic factors influencing the mechanism of *EET* between two chromophores is the key for the design and construction of efficient photonic devices and artificial energy harvesting systems that can be used, for example, in luminescent solar concentrators.¹⁰⁻¹² Multi-chromophore molecules, containing two or more distinguishable molecular units separated by bridges of controllable length, are ideal systems for investigating *EET* processes. The properties of the bridge determines the degree of flexibility of the whole structure and are responsible for the “*through bond*” energy transfer as well as *short range* interactions.¹³ Furthermore, the electronic properties of the bridge can modulate the electronic coupling between donor and acceptor. The distance between chromophores is, along with the structure flexibility, one of the key parameters controlling the rate and yield of energy transfer.

In recent past, there has been a remarkable effort, both from the experimental and theoretical point of view, in developing and analysing molecular systems able to perform efficient and rapid energy transfer upon light absorption.^{2, 6, 14-16} This provided a more detailed understanding both of the energy transfer mechanisms and of the key factors influencing their efficiency. The development of ultrafast non-linear spectroscopic methods and the increased computational capability, which nowadays allows to study with highly accurate *ab-initio* methods also systems of considerable size, certainly helped in this regard.

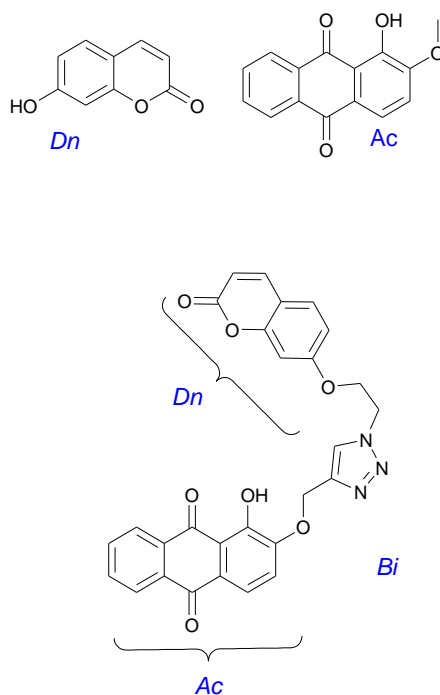
From a general point of view, the efficiency of intramolecular *EET* can be principally related to the magnitude of the coupling between donor and acceptor (V_{Dn-Ac}), which depends on their electronic structures and to the influence of the surrounding medium, which can modulate the molecular interactions. Depending on the relative magnitude of the electronic coupling and on the donor vibronic bandwidth, we can distinguish between *strong coupling*, *intermediate coupling* and *weak*

coupling EET regimes. In the strong coupling case, the excitation is delocalized on both donor and acceptor. A particularly challenging and intriguing problem regards the modelling of *EET* dynamics in the intermediate coupling case. In this case, relaxation of the external bath happens on the timescale of *EET*, and mixing of the donor and acceptor states can lead to coherent dynamics on short timescales.^{1, 2, 17, 18} On the other hand, within the weak coupling regime, the rate of energy transfer k_{ET} from *donor* to *acceptor* can be derived from the time-dependent perturbation theory and the Fermi Golden Rule as¹⁹⁻²¹

$$k_{ET} \sim |V_{Dn-Ac}|^2 (FCWD)$$

where FCWD represents the Franck-Condon weighted density of states, corresponding to the product of the densities of vibrational states in the initial and final electronic states of the system. The effective electronic coupling matrix element V_{Dn-Ac} can be expressed as a sum of terms,¹³ depending on the Coulomb interactions between dipoles and/or higher multipoles of donor and acceptor, and on the electronic properties of the connecting molecular bridge. In general, application of the Fermi Golden rule through the Foster expression results in a quite accurate estimate of the energy transfer rate in a large number of cases.^{20, 22}

The interplay between ultrafast spectroscopic methods and advanced theoretical modelling can give notable contribution to the comprehension of the mechanisms regulating the efficiency of EET in molecular systems. With this in mind, in this work we present the synthesis and the characterization of EET in a bichromophoric system constituted by two naturally occurring dyes: Umbelliferone (*Dn*) and Alizarin (*Ac*), whose structure is shown in Scheme 1.



Scheme 1: structure of *Ac* (right), *Dn* (left) and *Bi* (bottom).

Both the donor and acceptor molecules selected in our study are well known and commonly used dyes. Umbelliferone is a widespread natural product that belongs to the coumarin family; it is used in many different fields, for instance as a component in sunscreens, as optical brightener for textiles, as a gain medium for dye lasers and can be used as a fluorescence indicator for metal ions like copper and calcium. Alizarin has been used throughout history as a red dye, principally to colour textiles; it is the main ingredient for the manufacture of the madder lake pigments known to painters as *Rose madder* and *Alizarin crimson*.

We employed femtosecond transient absorption spectroscopy for the experimental characterization of the system, and investigated its electronic structure by means of density functional Theory (DFT) computations. One of the principal aims of this work was to verify if Förster model can still be applied in case of very fast kinetics, which, on a first sight, would suggest the occurrence of high electronic coupling between the donor and acceptor. In reality, other factors can determine the fast energy transfer rate, as for instance the coupling with the surrounding media, or the geometrical arrangement of the two chromophores. It is thus important to dispose of a computational protocol able to reproduce the electronic properties of the system, allowing both for a comparison with its experimental spectra and for the rationalization of its dynamic properties.

Our results demonstrate that in case of the analysed system, the electronic coupling between the donor and acceptor is weak, thus justifying the modelling of the energy transfer process through the dipole-dipole approximation. The structural flexibility of the system and the short distance between the donor and acceptor moieties determine the efficiency of energy transfer and its velocity. The EET kinetic constant obtained from the Förster expression is well comparable with the experimental one.

Methods

Synthetic procedures

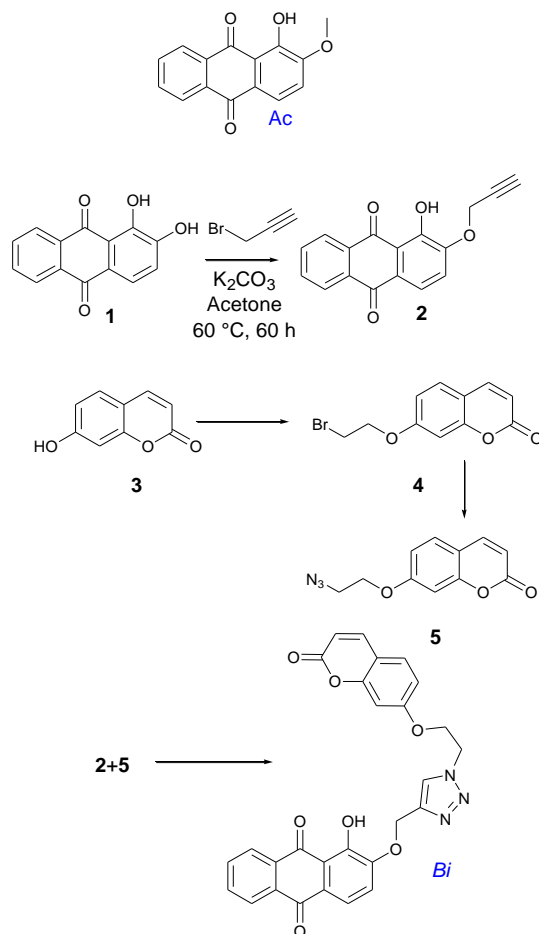
For the synthesis of compounds **Ac**^{23, 24}, **4**,²⁵ **5**²⁶ we followed synthesized following the procedures described in the pertinent literature.²⁷

Synthesis of 1-hydroxy-2-prop-2-ynyloxy-anthraquinone (2).

A 100 mL round bottomed flask was charged with Alizarin (**1**) (240 mg, 0.85 mmol), dry K₂CO₃ (629 mg, 5.9 equiv) and 40 ml of dry acetone to obtain a deep purple dispersion. Propargyl bromide (89 mL, 1 mmol, 1.2 equiv) was added and the dispersion was heated at 60 °C for 60 h. The solution was concentrated and the crude solid was added with CH₂Cl₂ (50 mL) and the resulting suspension was washed with 0.5 N solution of HCl (2 x 25 mL) and finally with brine (2 x 20 mL). The organic solution was dried over Na₂SO₄ and concentrated to afford an orange gummy residue. The crude

reaction mixture was purified by flash column chromatography to afford 54 mg of compound **2** (23% yield)

Compound **2**: $R_f = 0.22$ (CH_2Cl_2); $^1\text{H NMR}$ (200 MHz, CDCl_3): δ ppm 8.35-8.25 (m, 2H), 7.80 (d, $J = 7.1$ Hz, 1H), 7.72 (m, 2H), 7.45 (d, $J = 7.1$ Hz, 1H), 4.91 (d, $J = 2.1$ Hz, 2H), 2.63 (t, $J = 2.1$ Hz, 1H). Ms(EI, 70 eV): m/z (%) 278 (M⁺), 211, 183, 126, 77. Elemental analysis calculated for $\text{C}_{17}\text{H}_{10}\text{O}_4\text{-H}_2\text{O}$ (296.28), C 73.38, H 3.62, O 23.0. Found C 73.21, H 4.16.



Scheme 2: Schematic reaction steps for the synthesis of **Dn**, **Ac**, **Bi**.

Synthesis of compound **Bi**

A 10 mL round bottomed flask was charged with 7-(2-azido-ethoxy)-chromen-2-one (**5**) (100 mg, 0.43 mmol), 1-hydroxy-2-prop-2-ynoxy-anthraquinone (**2**) (120 mg, 0.43 mmol), $\text{CuBr}(\text{PPh}_3)_3$ (0.1 equiv), DIPEA (0.85 mL) and 4.5 mL of dry and degassed THF. The solution was left under stirring in inert atmosphere for 7 days. The solution was concentrated and the crude reaction mixture was purified by flash column chromatography to afford 74 mg of compound **Bi** (34% yield).

Compound **Bi**: $R_f = 0.25$ (CH_2Cl_2); $^1\text{H NMR}$ (400 MHz, $\text{DMSO-}d_6$, 60°C): δ ppm 8.34 (s, 1H), 8.26-8.23 (m, 1H), 8.21-8.18 (m, 1H), 7.96-7.92 (m, 3H), 7.70 (d, $J = 9.6$ Hz, 1H), 7.6 (d, $J = 9.6$ Hz, 1H), 7.57 (d, $J = 9.6$ Hz, 1H), 6.99 (d, $J = 2.4$ Hz, 1H), 6.8 (dd, $J = 9.6, 2.4$ Hz, 1H), 6.26 (d, $J = 9.6$ Hz,

1H), 5.36 (bs, 2H), 4.83 (t, $J = 4.8$ Hz, 2 H), 4.54 (t, $J = 4.8$ Hz, 2H). IR (KBr): 3339 (w), 2923 (m), 1802 (m), 1728 (m), 1268 (m) cm^{-1} . MS (EI, 70 eV): m/z 510 (M^{++1}), 466. Elemental analysis calculated for $\text{C}_{28}\text{H}_{19}\text{N}_3\text{O}_7$ (509,12), C, 66,01; H, 3,76; N, 8,25; O, 21,98. Found C 66.35, H 3.45, N 8.35.

Absorption and Fluorescence

The absorption and fluorescence spectra were recorded on Perkin Elmer *Lambda 950* spectrophotometer and a *LS-55* fluorometer, respectively. Fluorescence quantum yields were obtained by measuring the corrected area of samples and standards: Anthracene ($\Phi = 0.27$) for *Dn* and Rhodamine B ($\Phi_{340} = 0.7$, $\Phi_{440} = 0.5$) for *Ac* and *Bi*.²⁸

Time-resolved measurements

The experimental instrumentation and data processing for femtosecond time-resolved transient absorption spectroscopy have been described in detail in previous reports.²⁹⁻³² Briefly, ultrashort pulses (~ 100 fs, 800 nm, 1 kHz rep. rate, 700 $\mu\text{J}/\text{pulse}$) are produced by a regenerative amplified Ti:Sapphire laser system (BMI ALPHA 1000). A BBO-based optical parametric amplifier (TOPAS, LightConversion) provides tuneable excitation pulses. In the present experiment the excitation wavelength of 330 and 400 nm were obtained respectively as the fourth harmonic of the output (*Signal*) of TOPAS at 1320 nm, and as the second harmonic of a portion of the laser output. A small portion of the 800 nm beam was focused on a 2.5 mm thick calcium fluoride plate to generate the white-light continuum used for probing. The resulting spectrally broadened laser pulse spanned the entire visible region and extended in the near UV to roughly 325 nm. The white-light continuum was further split into two parts of equal intensity by a 50/50 fused-silica–Al beam splitter. One part, acting as the probe beam, was spatially overlapped with the excitation beam in the sample. The second part crossed the sample in a different position and provided a convenient reference signal. The probe and reference beams were spectrally dispersed in a flat-field 25 cm Czerny–Turner spectrometer, and detected by means of a back illuminated CCD camera with spectral response in the region 300–1000 nm. Two different configurations of the detection system were utilized to obtain the data sets herein presented, which are composed of both transient spectra (absorbance of the excited state versus wavelength at a given pump–probe delay time) and kinetic plots (intensity of the probe versus delay time at a fixed wavelength). Measuring kinetic plots requires narrow bandwidth detection. The desired wavelengths were selected with 5 nm bandwidth interference filters. The detection system for measuring the probe pulse intensity consisted of a silicon difference photodiode and a lock-in amplifier. The latter was synchronized to a chopper switching the pump pulse on and off at half the

repetition-rate of the laser system, yielding directly the differential spectrum of the probe. In every experiment the relative pump–probe polarization was set at the magic angle (54.7°) to discriminate against rotational dynamics. The reduced laser repetition rate (100 Hz) and the stirring of the sample by means of a micro magnet inside the cell prevented any photo-damage of the sample. The sample absorbance at the excitation frequency was in all cases between 0.6-0.8 OD for isolated chromophores, with excitation energies between 0.5-0.7 $\mu\text{J}/\text{pulse}$.

Time-resolved data Analysis

The time-resolved spectra were corrected for the group velocity dispersion (GVD) of the probe pulse; optical Kerr measurements on the same solution employed in the transient absorption experiment provided the GVD curve. We analysed the transient signal in the time domain with the help of a home developed global fitting program. The time domain signal can be reproduced as the convolution of the appropriate molecular response function with the instrumental function *IRF* (the cross-correlation between pump and probe pulses). It was obtained from the time profile of the Stimulated Raman Gain (SRG) signal of the solvent: 330 nm excitation pulses produce *IRF* of 300 fs FWHM, while 200 fs FWHM is obtained with 400 nm excitation. The molecular response function for global data analysis of isolated *Dn* and *Ac* has the form

$$R_\lambda(t) = \sum A_i^\lambda \exp^{-t/\tau_i} \quad (1)$$

The λ subscript indicates that the pre-exponential factor depends on the probed wavelength, while the exponential is wavelength-independent. The global fitting method consists of the simultaneous simulation, with the same kinetic model, of multiple decay traces, usually distributed on the whole spectral range of interest. This method allows the accurate determination of the decay constants, the number of equations available being substantially larger than that of the time constants to be determined.

For the simulation of the kinetic traces of *Bi* we adopted a different model which takes into account the transfer process. For the short time part (up to 5 ps) of the kinetic traces we used the convolution of the *IRF* with a molecular response function given by:

$$R_\lambda(t) = A_0^\lambda + A_{ET}^\lambda (1 - \exp^{-t/\tau_{ET}}) \quad (2)$$

where A_0 accounts for the amount of direct excitation of the acceptor unit, while A_{ET} represents the energy transfer component. The decay of the kinetic traces was fitted with a bi-exponential function:

$$R_\lambda(t) = A_1^\lambda \exp^{-t/\tau_1} + A_2^\lambda \exp^{-t/\tau_2} \quad (3)$$

where τ_1 is related to the vibrational cooling, while τ_2 represents the electronic relaxation.

Computational details

Ground state equilibrium structures were calculated for the isolated ***Dn***, ***Ac*** and for ***Bi***. In order to characterize the different possible conformations we investigated several local minima of the potential energy surface (PES). The calculated vibrational frequencies confirm that the optimized structures correspond to local energy minima: all structures considered have only positive eigenvalues of the Hessian matrix. All the computations were performed using the GAUSSIAN09 program package³³ with the density functional theory (DFT) approach. We employed the CAM-B3LYP³⁴⁻³⁷ functional and the *aug*-N07D basis set,³⁸ as this combination has been shown to give accurate results in the modelling of spectroscopic properties of medium to large systems.³⁹⁻⁴¹ We included the solvent effects by means of the conductor-like polarizable continuum model (CPCM),⁴²⁻⁴⁴ using the default parameters to define the cavity. The free energy computation at T=298.15 K and p=1 atm take into account the dispersion, repulsion^{45, 46} and cavitation energies⁴⁷, using Boltzmann statistic for the evaluation of the relative abundances of the different conformations. We adopted the time-dependent density functional theory (TD-DFT)^{48, 49} for the simulation of the absorption and emission electronic spectra of all systems, using the B3LYP functional and *aug*-N07D basis set. Vertical excitation energies (VE) and energy gradients were computed for the excited electronic states on the ground-state equilibrium geometry, including the environmental effects by means of the CPCM with the VE computed with the linear response LR-PCM/TD-DFT approach within the non-equilibrium solvation regime.⁵⁰⁻⁵³ We simulated the vibrationally resolved electronic spectra by means of a procedure based on the selection and computation of the relevant overlap integrals between the vibrational wavefunctions of the electronic states involved in the transition⁵⁴⁻⁵⁷, adopting the vertical gradient (VG) approach. The basic assumption is that the PES in the excited state retains the same shape as in the ground state, apart from a shift of the equilibrium position, which is calculated from the TD-DFT gradients at the ground state geometry. Moreover, it is assumed that the initial and final states' normal modes are the same and that the harmonic vibrational frequencies remain unchanged. This description of the final state PES, without its explicit calculation, reduces considerably the computational cost, allowing us to compute the absorption and emission spectra of all the states of the bi-chromophoric systems in all the relevant conformations. Such an extensive study was aimed at investigating possible different behaviours of the different conformations and it would have been unfeasible with more accurate models of the excited PESs. However, the reliability of our analysis is supported by the fact that the VG approach is well-suited for the simulation of the general shape of low-resolution spectra in solution, and it is particularly advocated in the absence of significant changes of the geometrical parameters during the electronic excitation and whenever the harmonic approximation is valid.^{58, 59}

Due to the brightness of the relevant states for EET, we performed all computations within the Franck-Condon (FC) approximation,^{60,61} by considering only the constant zero order term in the Taylor series expanding the dipole moment as a function of normal coordinates. In order to simulate FC|VG absorption spectra, only the harmonic frequencies at ground state equilibrium geometry and vertical excitation energy gradients need to be calculated. For each system, we obtained the final FC|VG spectra by summing the singlet-state transition of all excited electronic states considered, without accounting for the temperature effects. The same data utilized for computing the FC|VG absorption spectra were used to simulate the emission spectra. This procedure, adopted for its computational convenience, introduces additional inaccuracies, because the initial and final electronic PES are not expanded around the excited-state equilibrium geometry, i.e. the FC region for the emission process. Stick spectra were convoluted by means of Gaussian functions with half-width at half-maximum (HWHM) equal to 800 cm^{-1} , this value being chosen to reproduce the experimental line-shapes. It is noteworthy that an *a priori* estimate of the inhomogeneous broadening from the solvent reorganization energy (see Ferrer and co-workers⁶² for details) predicts for **Dn** an extremely similar value i.e. 765 cm^{-1} . The same calculation for **Ac** gives an *a priori* HWHM of 1090 cm^{-1} . In all computations were used a locally modified version of the Gaussian suite of programs.

Results

Static measurements

Derivatives of hydroxyl-coumarin are known to be characterized by large frequency shift of emission and absorption bands in dependence of the solution's pH. Particular attention has been devoted to the characterization of 7-Hydroxy-4-methylcoumarin (7H4MC) and 7-Hydroxycoumarin (7HC) in the ground singlet S_0 and first singlet S_1 excited states. Several authors investigated the behaviour of these compounds in different solvents and pH conditions by means of static⁶³⁻⁶⁷ and time-resolved^{65, 68-70} spectroscopic techniques, concluding that in polar *non*-protic solvent (like acetonitrile) the absorbing and emitting specie is the neutral form. The absorption spectrum, Fig. 1, consists of an intense band centered at 320 nm ($\epsilon \sim 13000\text{ M}^{-1}\text{ cm}^{-1}$), while the fluorescence spectrum obtained with 330 nm excitation shows a broad and unstructured band centered at 380 nm ($\Phi_{Dn}=0.011$). Several authors investigated the steady state properties of Hydroxy-anthraquinone (HAQ) derivatives using different spectroscopic techniques.^{71, 72} One of the most important properties associated to the HAQ is the ability to give intramolecular proton transfer in the excited state. The tautomeric reaction takes place in the S_1 electronic state and only the 9,10 -CO and 1,4,5,8 -OH functional groups are involved in the process. The *excited state intramolecular proton transfer* (ESIPT) reaction induces a large

change of the electronic configuration of the molecule resulting in dual emission (normal and tautomeric) that, since Weller's studies on methyl salicylate,^{73,74} has been used as a marker to identify

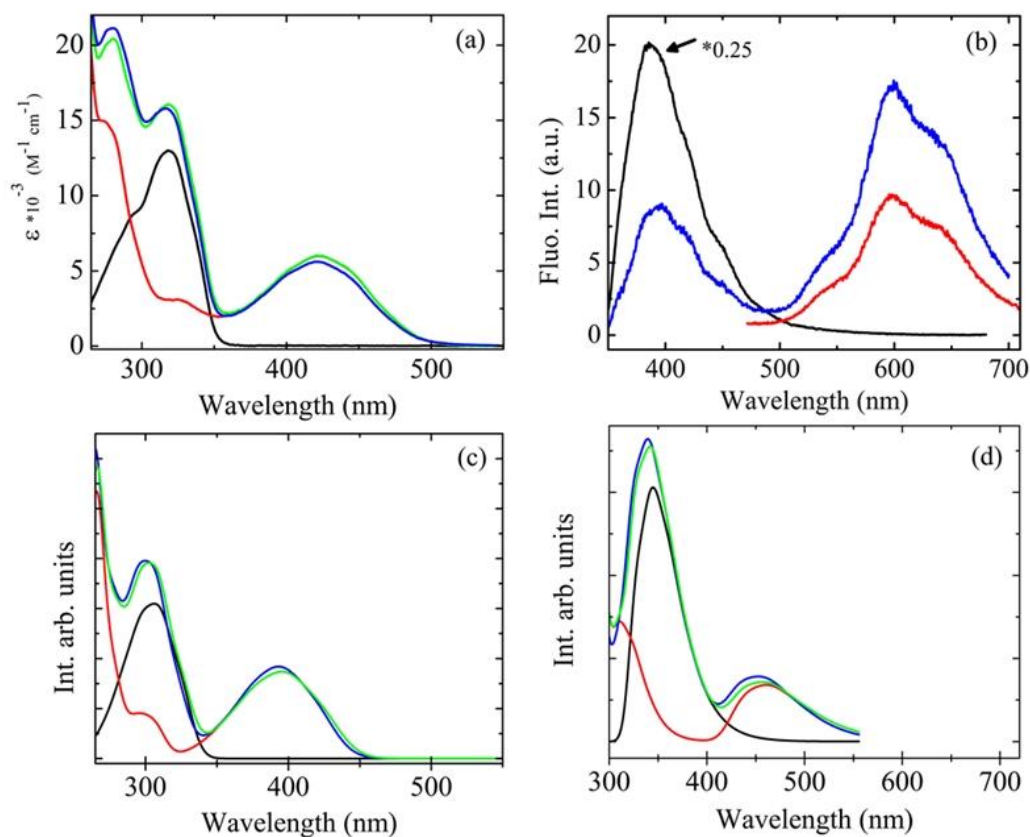


Fig. 1

(a) Molar absorption coefficients of **Dn** (black), **Ac** (red), **Bi** (blue) and the sum **Dn+Ac** (green). (b) Fluorescence spectra of **Dn** (black), **Ac** (red) and **Bi** (blue). Calculated vibrational resolved electronic absorption (c) and emission (d) spectra of **Dn** (black), **Ac** (red), **Bi** (blue) and the sum **Dn+Ac** (green).

the ESIPT process. Owing to the ESIPT in the excited singlet-state, an enol-tautomer is converted to a keto-one, and a largely Stokes-shifted fluorescence appears.⁷⁵ The experimental absorption and fluorescence spectra are shown in Fig.1, upper panels. The absorption maximum is located at 420 nm with $\epsilon = 5950 \text{ M}^{-1}\text{cm}^{-1}$. The fluorescence emission is centred at 620 nm and, with 400nm excitation, has a quantum yield $\Phi^{400}_{Ac} = 0.0045$. We determined also the fluorescence quantum yield with 330 nm excitation, i.e. exciting in the spectral region where the $S_0 \rightarrow S_1$ and $S_0 \rightarrow S_2$ absorptions are overlapped, obtaining $\Phi^{330}_{Ac} = 0.0042$.

The absorption spectrum of **Bi**, Fig.1, is very well reproduced as the sum of **Dn** and **Ac** spectra, what suggests that the electronic interaction between **Dn** and **Ac** in the ground state is weak. If we use the sum spectrum **Dn+Ac** as a reference, we observe a slight hypsochromic shift of the $S_0 \rightarrow S_1$ transition and a weak hypochromism on all the absorption bands. The fluorescence quantum yield, with 400 nm excitation, is $\Phi^{400}_{Bi} = 0.005$, a value comparable, within the experimental error of 10-15%, to the 10

quantum yield of isolated **Ac**. To determine the amount of energy transfer we measured the quenching of the fluorescence of **Dn** in the presence of the acceptor.⁷⁶ We notice that the excitation at 330 nm is not a “pure” excitation, because both the **Dn** and **Ac** units absorb at this wavelength. However, as the absorption cross-section of **Bi** is very well approximated by the sum of **Dn** and **Ac**

$$\varepsilon_{Bi}(\nu) \cong \varepsilon_{Dn}(\nu) + \varepsilon_{Ac}(\nu) \quad , \quad (4)$$

we can calculate the relative weight of the two cross-sections at $\nu_1 = 330 \text{ nm}$:

$$\begin{aligned} \alpha_{Dn}(\nu_1) &= \frac{\varepsilon_{Dn}(\nu_1)}{\varepsilon_{Bi}(\nu_1)} \\ \beta_{Ac}(\nu_1) &= \frac{\varepsilon_{Ac}(\nu_1)}{\varepsilon_{Bi}(\nu_1)} \end{aligned} \quad (5)$$

If we assume that the excitation is divided into the two sub-units according to their cross-sections ratio, then we can easily calculate the corrected fluorescence quenching and fluorescence enhancement of **Dn** and **Ac**. Being the fluorescence quantum yield of **Dn** in **Bi** $\Phi'_{Dn}=0.0016$, we calculate the transfer efficiency from the relation

$$E = 1 - \frac{\Phi'_{Dn}}{\Phi_{Dn}} \quad (6)$$

where Φ'_{Dn} and Φ_{Dn} are the donor quantum yields with and without the acceptor, obtaining $E=86\%$. This experimental evidence demonstrates that the transfer efficiency is quite high; what is left to understand is the mechanism of the energy transfer and the kind of interaction established between the two chromophoric units, a key factor in the intra-EET process. We followed two distinct approaches to answer the two former questions. From one side we performed quantum chemical calculations on the ground and excited state of both the bichromophore and the isolated **Dn** and **Ac** to characterize the distribution of electron density; from the other side we measured the energy transfer rate constant k_{et} by means of femtosecond transient absorption spectroscopy.

Time-resolved measurements

The spectra of the isolated **Dn**, corrected for the GVD effect are shown in Fig.2. We can easily recognize an excited state absorption (ESA) band centred at 355 nm and a stimulated emission (SE) band at 405 nm (Fig.4 left panel). There is also evidence of a broad absorption band, compared to the 350 nm ESA, on the low frequency side of the SE band.

Single wavelength experiments were performed to measure the time evolution of the main spectral features. We selected four different wavelengths: 405, 450, 500 and 550 nm and performed the acquisition in the same experimental conditions used to record the transient spectra. We repeated the

measurements on different days and on different samples in order to guarantee the reproducibility of the data.

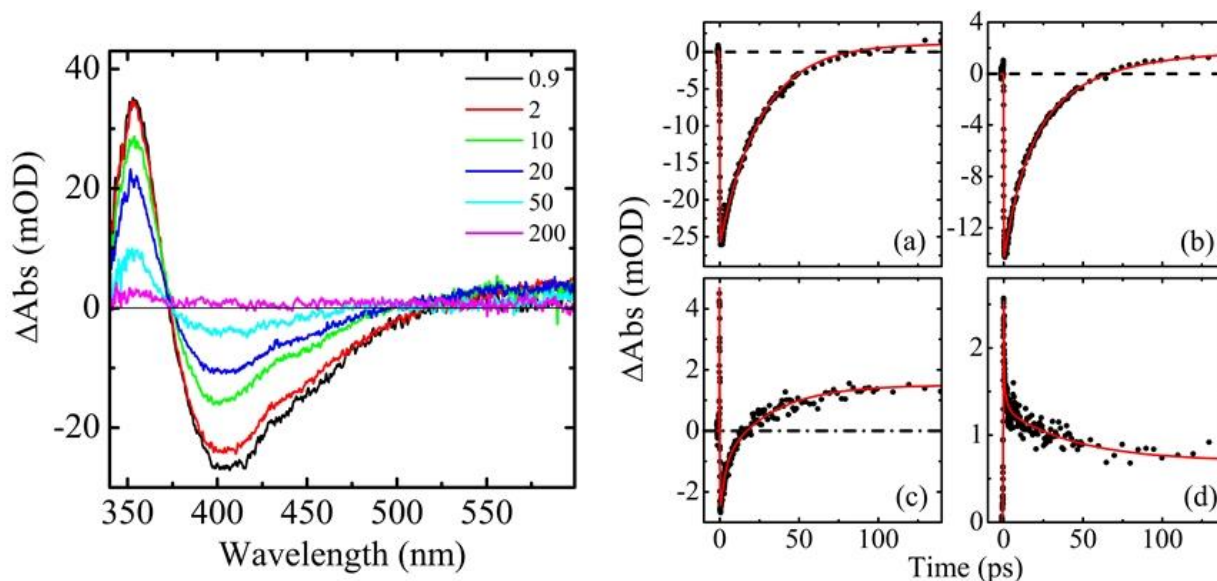


Fig. 2

Left panel Transient spectra of isolated **Dn** at selected delays (ps) $\lambda_{\text{exc}}=330$ nm. *Right panel* Kinetic traces (scatter) and fitting curve (red line) recorded with probe wavelength (a) 400 nm, (b) 450 nm, (c) 500 nm and (d) 550 nm.

We assumed the sum of three exponential functions plus a constant as the model function used in the data analysis. The first exponential reproduces the cross-phase modulation artefact (XPM) that affects the first 100 fs.⁷⁷⁻⁷⁹ Transient absorption and stimulated emission bands grow-up with the same rise time that, taking into account the XPM, is comparable with our temporal resolution. This means that they are associated to transitions occurring from the same excited state and that the excitation of **Dn** with $\lambda_{\text{exc}} = 325$ nm directly populates the first singlet excited state (S1). The other two exponential functions used to fit the kinetic data have time constants of 3 ps and 27 ps. The first component represents the vibrational relaxation in the S1 excited state, while the second is directly related to the depopulation of S1. S1 is completely depopulated 200 ps after the excitation, but, as shown in Fig.2, the transient signal does not go to zero on the experimentally accessible time scale (maximum delay 1.8 ns). After 200 ps all the kinetic traces show a transient absorption signal with constant intensity in the whole inspected temporal window. This behaviour can be explained by the presence of a lower energy excited state, which is populated during the decay of the S1 excited state. Static and time-resolved studies^{69, 70, 80} were previously carried-out to characterize the behaviour of 7H4MC and 7-methoxy- 4-methylcoumarin (7Met4MC) on the microsecond time scales. All the authors agree that both chromophores have an excited triplet T1 state that is populated after the decay of S1. This led

us to conclude that the S1 excited state population of 7HC rapidly decays by internal conversion, fluorescence emission and by inter-system crossing (ISC) towards the first triplet excited state T1. The characterization of the excited state dynamic of the isolated **Ac** is a fundamental step for the comprehension of the energy transfer process in the **Dn-Ac** compound. We excite **Ac** with 330 and 400 nm pulses, corresponding to the blue side and almost to the centre of the S0→S1 transition, respectively. The ESIPT is the fundamental event following the S0→S1 excitation and it is indirectly promoted by the energy transfer in the bichromophoric system. Since also **Ac** absorbs in the 400 nm region, it is essential to characterize the response of the isolated **Ac** to excitation at this wavelength in order to extrapolate the contribution of the direct excitation in the bichromophore.

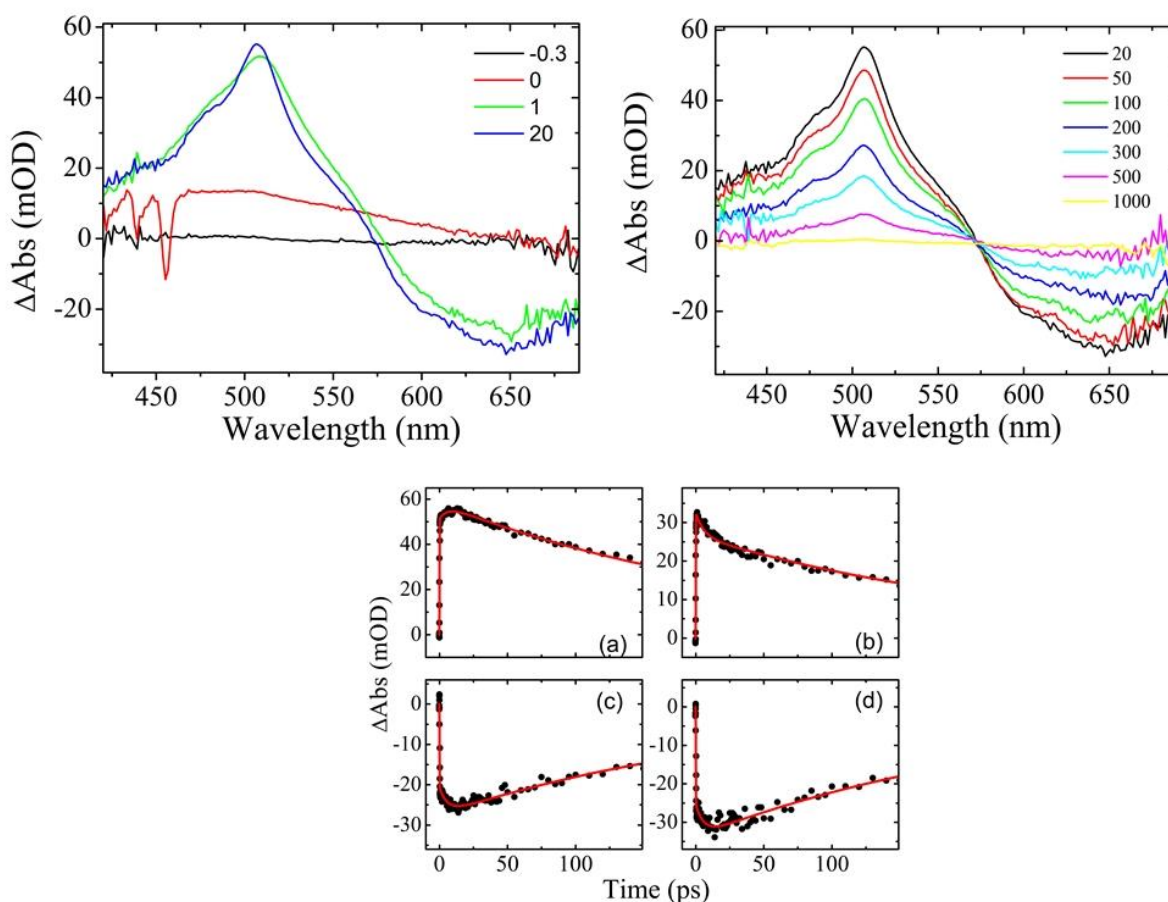


Fig. 3

Upper panel Transient spectra of isolated **Ac** at selected delays (ps), $\lambda_{\text{exc}}=400$ nm. *Lower panel* Kinetic traces (scatter) and fitting curves (red line) of isolated **Ac**, $\lambda_{\text{exc}}=400$ nm, recorded at (a) 510, (b) 535, (c) 620 and (d) 650 nm.

The left panel of Fig.3 shows the spectral evolution of **Ac** during the first twenty picoseconds after 400 nm excitation. The spectrum at "zero" delay time is characterized by XPM, while the main features observed at positive delays are the excited state absorption (ESA) and the stimulated emission (SE) bands centred at 508 nm and 600 nm, respectively. The ground state bleaching (GSB)

expected in the blue side of the spectra is completely covered by the intense and broad ESA. The ESA band is broader and its vibronic structure is less pronounced in the spectrum recorded at 1 ps compared to the spectrum recorded at 20 ps. This is the consequence of the vibrational relaxation. Immediately following the excitation event the electronic population is localized on excited vibrational levels of the S1 state (Franck-Condon principle). The excess of vibrational energy is then redistributed on the various normal modes or dissipated through collisions with the solvent molecules. The vibrational relaxation involves changing of the Franck-Condon factors associated to the transitions from the excited state and, consequently, of the intensity and shape of the bands of the transient spectrum. Typical effects of the vibrational relaxation are line narrowing and intensity increase of the transient absorption and stimulated emission bands⁸¹⁻⁸³; a blue shift of the band maximum is commonly observed too. The spectra recorded at longer delay times are collected in the right panel of Fig.3; they show that the ground state recovery is complete in 1 ns. Single wavelength measurements (Fig.3, lower panels) were recorded at 510, 535, 620 and 650 nm following the procedure previously described. All the kinetic traces were well reproduced by the convolution of the *IRF* with the sum of two exponential functions with time constants $\tau_1=7 \pm 1$ ps and $\tau_2=238 \pm 5$ ps. The excited state S1 decays with τ_2 , while the first time constant represents the vibrational relaxation (VR) within S1 potential well. In our transient spectra we cannot observe any dynamics attributable to the proton transfer; all the transient spectra belong to the excited state of the enol-form. This is consistent with the ultrafast (~ 50 fs) nature of the ESIPT process reported in literature for Anthraquinone.⁸⁴⁻⁸⁹ Excitation with 330 nm pump pulses results in transient spectra and kinetic traces completely analogous to the ones obtained with 400 nm excitation. The time constants, assuming a bi-exponential molecular response function, are $\tau_1=8 \pm 1$ ps and $\tau_2=240 \pm 5$ ps. The transient spectra and the comparison between the kinetic traces recorded with $\lambda_{exc}=330$ nm and $\lambda_{exc}=400$ nm are shown in Supplementary Information (figure S1 and S2).

Transient spectra of **Bi** show the main features of **Ac**: the ESA band centered around 508 nm, and the SE band centered at 650 nm. The quality of the spectra is lower respect to those recorded on the isolated **Ac** because the solubility of **Bi** is very low, so that the maximum achievable absorbance at the excitation frequency was 0.2/0.3 OD.

However, the shape of the high frequency side of the ESA band differs from that of the isolated acceptor (see Fig. 4). As we showed in Fig. 2, the excited state spectra of **Dn** are characterized by the SE at 400 nm and by an intense ESA centered around 350 nm. Hence, in the spectral region between 350 and 420 nm, the transient spectra of **Bi** consist of the sum of more than one contribution: namely, the residual ESA and SE of **Dn**, plus the broad ESA of **Ac**. This effect is particularly evident in the spectra shown in the upper left panel of Fig.4.

The spectra reported in Fig.4 clearly show a different temporal evolution in the region between 450 and 650 nm with respect to **Ac**. In particular, it is evident a slower rise-time of the *ESA* and *SE* in respect to the isolated acceptor which shows only an increase and a slight blue shift of the *ESA* band maximum.

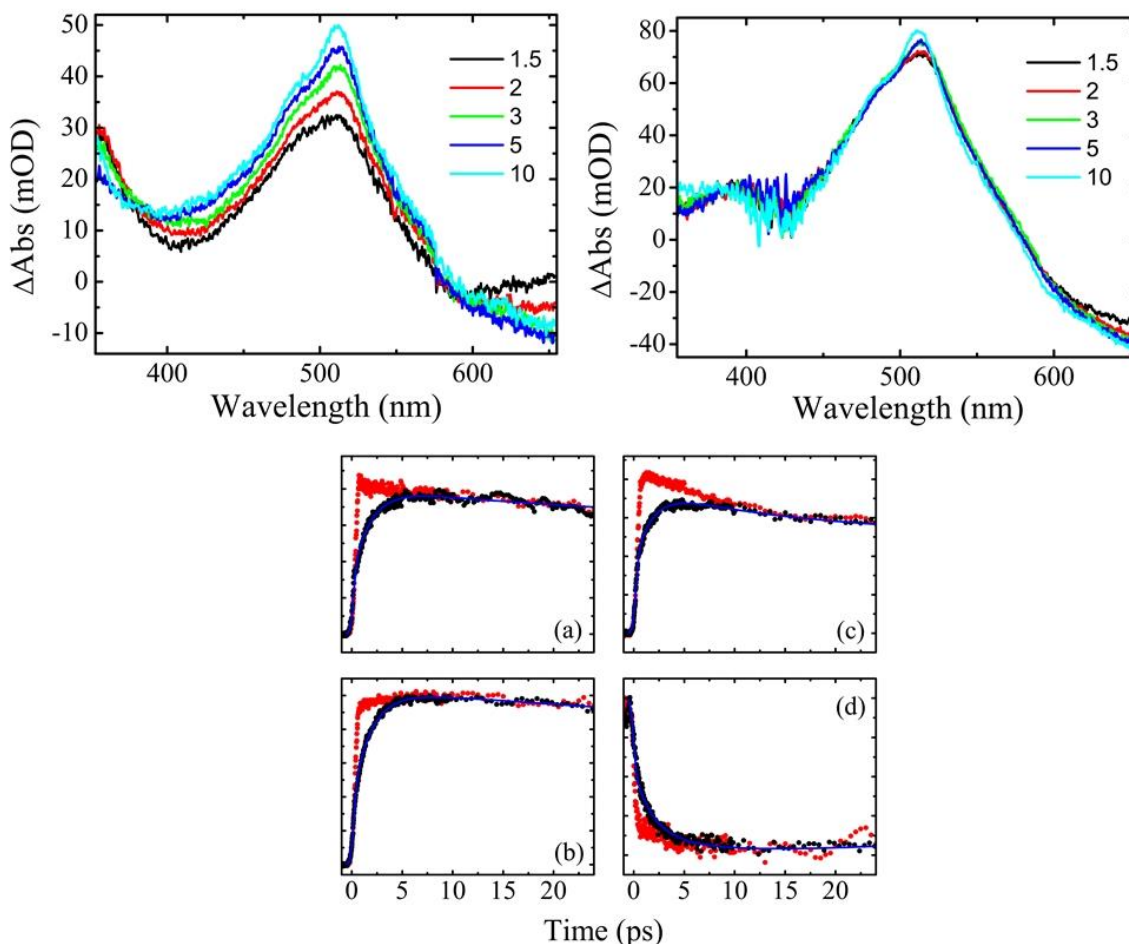


Fig. 4

Transient spectra of **Bi** (Upper left panel) and isolated **Ac** (Upper right panel) at selected delays (ps) $\lambda_{exc}=330$ nm. (Lower panel) Normalized selected kinetic traces (a) 480, (b) 510, (c) 535 and (d) 635 nm, of isolated **Ac** (red scatter) and **Bi** (black scatter), $\lambda_{exc}=330$ nm. The blue line represents the fitting of the kinetic traces of **Bi**.

As we emphasized in the analysis of the **Ac** data, the blue shift is due to vibrational cooling. On the contrary, the slower rise is an indication that a second channel creates population in the excited state localised on then **Ac** unit: this is the evident marker of energy transfer between **Dn** and **Ac**. We report the kinetic traces and the fitting curve in Fig. 4. We modelled the data with the response functions described in equation 2 and 3, so that we can extract directly the energy transfer time constant $\tau_{ET} = 1.6 \pm 0.5$ ps. Vibrational relaxation and decay of the electronic excited state have, respectively, $\tau_1 = 8 \pm 1$ and $\tau_2 = 236 \pm 5$ ps. All the time constants obtained by analyzing the kinetic traces of **Dn**, **Ac** and **Bi** are summarized in Table 1.

Table 1. Time constant used for the simulation of kinetic traces of *Dn*, *Ac* and *Bi*.

λ_{exc} (nm)	<i>Dn</i>		<i>Ac</i>			<i>Bi</i>	
	τ_2 (ps)	τ_3 (ps)	τ_1 (ps)	τ_2 (ps)	τ_{ET} (ps)	τ_1 (ps)	τ_2 (ps)
330	3 ± 0.5	27 ± 2	8 ± 0.5	240 ± 5	1.6 ± 0.5	8 ± 0.5	236 ± 5
400	-	-	7 ± 0.5	238 ± 5	-	-	-

Computational results

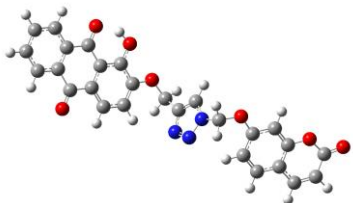
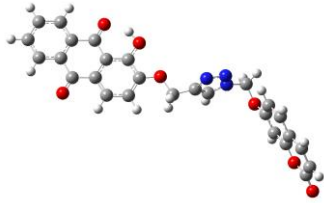
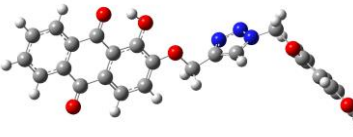
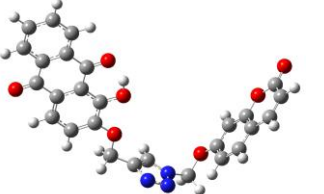
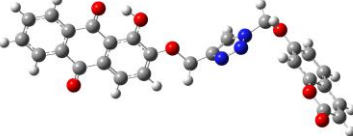
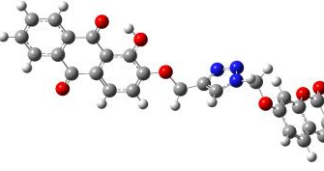
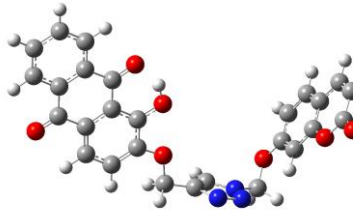
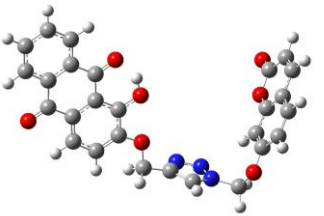
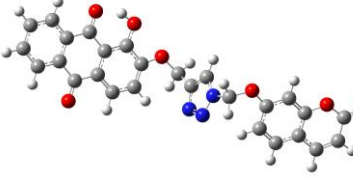
Conformational Analysis

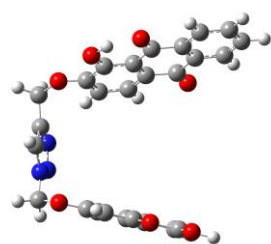
We started with the conformational analysis of *Dn* and *Ac* individually in order to simulate their absorption and emission spectra and to build the *Bi* structure, see scheme 1. The optimized geometry of the *Dn*, i.e. 7HC, is planar as expected. Indeed, this planar conformation favours the occurrence of stabilizing extended electronic delocalization, similar to other aromatic cyclic structures. As observed in previous works on Coumarin derivatives,⁹⁰⁻⁹² the OH substituent lies in the same plane as the whole molecule. From DFT calculations with the solvent effect embedded using the CPCM method, the conformation with the hydrogen in the OH group oriented towards the oxygen atoms of the pyranone ring is only 0.30 kJ/mol higher in energy than the conformation with the hydrogen at the opposite side; the two structures are then equally probable. No local minima were found corresponding to non-planar conformations.

The 1-Hydroxy-2-methoxy-anthraquinone (1-H2-MAQ) in acetonitrile was studied to model the *Ac*. Similarly to *Dn*, also in this case the equilibrium geometry is planar, with the C atom of the methoxy group (Cm) on the same plane defined by the anthraquinone atoms. Both the orientations of the hydrogen of the hydroxy group on the same and on the opposite side with respect to the methoxy group correspond to local minima, but the Gibbs free energy (ΔG) of the first orientation is more than 300 kJ/mol higher than that of the second one. Therefore, only the latter, from now on called 1C, will be considered in the following analysis. In addition, we investigated the conformations in which the hydrogen is shifted on the oxygens of the pyranone ring. The 1-9-form of quinone and the 1-10-quinone (with the hydrogen at the opposite site with respect to the methoxy group) are local minima, but both are again significantly less stable than 1C (free energy higher by 137 kJ/mol and 98 kJ/mol, respectively). Similar to previous DFT studies on 1-HAQ,⁹³ also our investigation leads to the conclusion that the geometry optimization of the 1,10-quinone form, with the hydrogen oriented towards the methoxy group, always converges to the 9,10-quinone structure. Another local minimum

(1D) was found for the conformation with the Cm lying outside the anthraquinone plane, and a C1-C2-O-Cm dihedral angle equal to -73 degrees. In this structure, which has an energy higher than the planar conformation 1C by 11 KJ/mol, one of hydrogen atoms of the methoxy group is oriented towards the oxygen of the hydroxy group. The analysis of the Boltzman populations leads to the conclusion that 1C is the dominant structure (98.5%) with a minor contributions of 1D (1.5%). The statistical weight of the other conformations is null (supp. Info).

Table 2: Calculated geometries of the most stable structures of the bichromophoric compound in acetonitrile: selected geometrical data, relative free energies in kJ/mol and Boltzmann populations.

	4C $\alpha = -75, \beta = -63$ $\gamma = -64, \varepsilon = 80$ $\Delta G = 7.35$ P% = 1.4		5C $\alpha = -180, \beta = -97$ $\gamma = -65, \varepsilon = -80$ $\Delta G = 0.00$ P% = 26.6
	6C $\alpha = 180, \beta = -93$ $\gamma = 63, \varepsilon = 79$ $\Delta G = 2.79$ P% = 8.6		7C $\alpha = -179, \beta = -92$ $\gamma = 66, \varepsilon = 73$ $\Delta G = 2.99$ P% = 8.0
	8C $\alpha = -179, \beta = -92$ $\gamma = -64, \varepsilon = -79$ $\Delta G = 1.10$ P% = 17.1		9C $\alpha = 180, \beta = 64$ $\gamma = 66, \varepsilon = 80$ $\Delta G = 1.55$ P% = 14.2
	10C $\alpha = -179, \beta = -96$ $\gamma = 66, \varepsilon = 80$ $\Delta G = 2.38$ P% = 10.2		12C $\alpha = 179, \beta = 93$ $\gamma = -66, \varepsilon = -79$ $\Delta G = 2.02$ P% = 11.7
	18C $\alpha = -76, \beta = -64$ $\gamma = -64, \varepsilon = -79$ $\Delta G = 7.66$ P% = 1.2		19C $\alpha = -76, \beta = -65$ $\gamma = -64, \varepsilon = -79$ $\Delta G = 8.83$ P% = 0.8



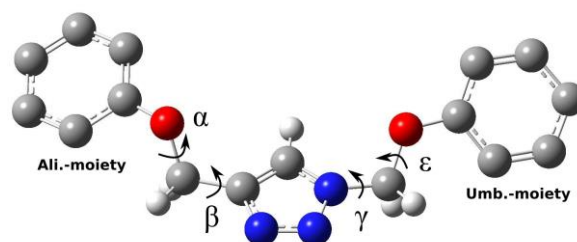
AAC

$$\alpha = -78, \beta = -64$$

$$\gamma = 61, \varepsilon = 75$$

$$\Delta G = 11.00$$

$$P\% = 0.3$$



We obtained the structure of **Bi** by connecting the optimized structures of **Ac** and **Dn** with the five atoms bridge. Starting from different initial positions of the two chromophores, we explored the PES through energy scans along selected internal coordinates, followed by geometry optimization. The most stable conformers of **Bi** in acetonitrile are shown in Table 2, together with relative energies and Boltzmann statistical weights. The five-atom bridge breaks the aromaticity and then the planarity. The rotations around the four dihedral angles shown in Table 2 define different stable orientations of **Ac** and **Dn**. The most stable conformer is 5C, with Boltzman population of about 25%. It is characterized by an open structure with respect to the position of the two chromophores, which are at opposite sides with respect to the bridge ring plane, at a distance (between the centres of mass) of about 14 Å. The plane of **Dn** is perpendicular to the one of **Ac** moiety. The other conformers with a relevant statistical weight (energies within 1.10-2.38 kJ/mol and Boltzman populations of 10-17%) are 8C, 9C, 10C, 12C. Also in all these cases, the planes of the two different chromophores are in an orthogonal position. Conformers 8C and 9C are quite similar to 5C. Otherwise, in 10C and 12C **Ac** and **Dn** are on the same side with respect to the bridge plane, at a distance of about 10 Å. Only the AAC conformer shows the two chromophores in a parallel face-to-face arrangement. With a statistical weight that does not exceed 1%, in this conformation the two chromophores are at the smallest distance, i.e. 7.5 Å.

Vibrationally resolved electronic spectra

We first calculated the electronic absorption and emission spectra for all **Dn** and **Ac** relevant conformations. Vibrationally resolved spectra were obtained by exploiting the procedure described in the computational details section. The most apparent result is that the calculated spectra of the different conformers in acetonitrile are practically indistinguishable. This observation suggests that the electronic structures of **Ac** and **Dn** chromophores in **Bi** are essentially decoupled, independently of the conformation. For this reason, from now on we will refer simply to the spectra of **Dn** and **Ac**, irrespective of the relative geometry in **Bi**. In Fig. 1 we present the experimental and calculated spectra of the individual chromophores and of the bichromophoric molecule.

For *Dn* in acetonitrile the absorption band in the spectral zone of interest, centred around 310 nm (red line in Fig.1) is due to the transition to the first electronic excited state, which is well represented by the $\pi \rightarrow \pi^*$ HOMO-LUMO transition. The two absorption bands of *Ac* (same figure, red line) originate from the transition to its first and second electronic excited states; the first one, centred on 390 nm, is due the $\pi \rightarrow \pi^*$ HOMO-LUMO transition. The 3D plots of frontiers orbitals, see Fig. S3, show that HOMO is located on the ring linked with the methoxy group, while LUMO is delocalized on all the atomic orbitals (AO) of the rings. On the other hand, the less intense band centred on 300 nm is mostly due to the HOMO-2 \rightarrow LUMO transition. The HOMO-2 is as well a localized orbital, with the electronic density located on the opposite side of the molecule with respect to the HOMO. Moreover, there is a small contribution due to the HOMO-4 \rightarrow LUMO+1 and the HOMO-2 \rightarrow LUMO+2 transitions, which are completely delocalized over the whole system. The simulated absorption spectra of both *Dn* and *Ac* are in very good agreement with the experimental ones, shown in the upper left panel of Fig.1. They present a slight hypsochromic shift (20-25 nm) with respect to the experimental spectra, but in general the shape of all bands and the relative intensities are remarkably well reproduced.

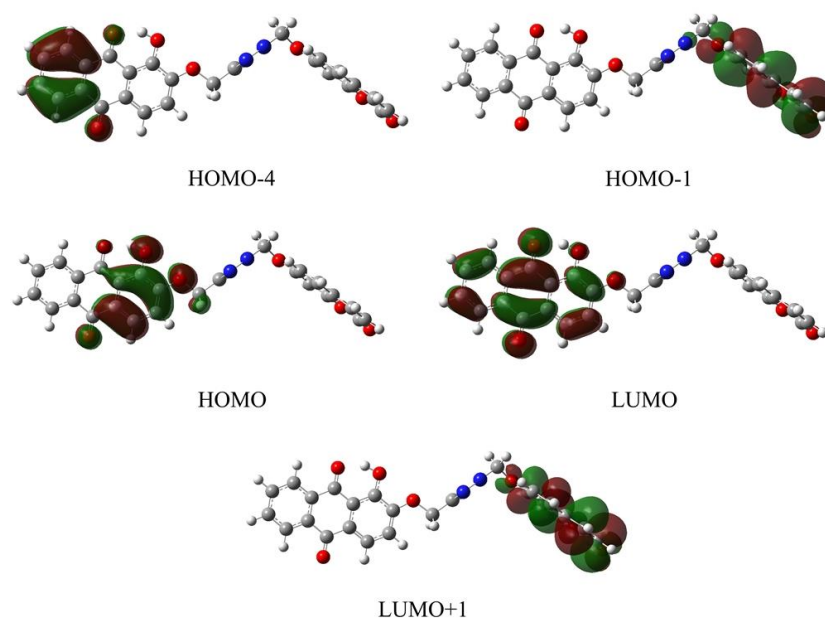


Fig. 5

3D plots of relevant MO of 5C conformer.

The emission spectra of *Dn* and *Ac* in acetonitrile are shown on the right panel of Fig.1. For *Dn* the computed band maximum is at 350 nm, shifted towards lower energies with respect to the experimental value by 30 nm. For *Ac*, the computed emission band maximum is at 470 nm, with respect to the 620 nm value observed experimentally. This difference is due to failure of the VG

approach in the case of the alizarin moiety. As discussed in the methodological section, this method is expected to deliver acceptable results only when the molecular system under study is not subject to relevant geometrical changes during the excitation. The ESIPT process in alizarin leads to a significant change of its geometry that cannot be well reproduced with our approach. In order to get a better agreement with the experiment, we performed TD-DFT optimization of the first excited electronic state of *Ac*. In Fig.S3 (see Supplementary Information) we report the ground and first excited electronic state structures of *Ac*. The proton shift leading to the 1-9 form of the quinone, is recovered. Taking into account only the VE, the LR-PCM/TD-DFT calculation at the excited state geometry gives an excitation energy of 560 nm, in better agreement with the experimental results. In this case we used the state-specific approach (SS-PCM/TD-DFT) to further improve the description of the solvent during the emission event. Here the apparent charges of the solvent are equilibrated with the true excited state charge density and not with the transition charge density, as it happens in LR-PCM.^{94, 95} Within the *External-Iteration* standard SS procedure implemented in the most recent release of Gaussian 09,⁹⁶ the VE is 569 nm, a result showing a further improvement of the agreement with the experimental value.

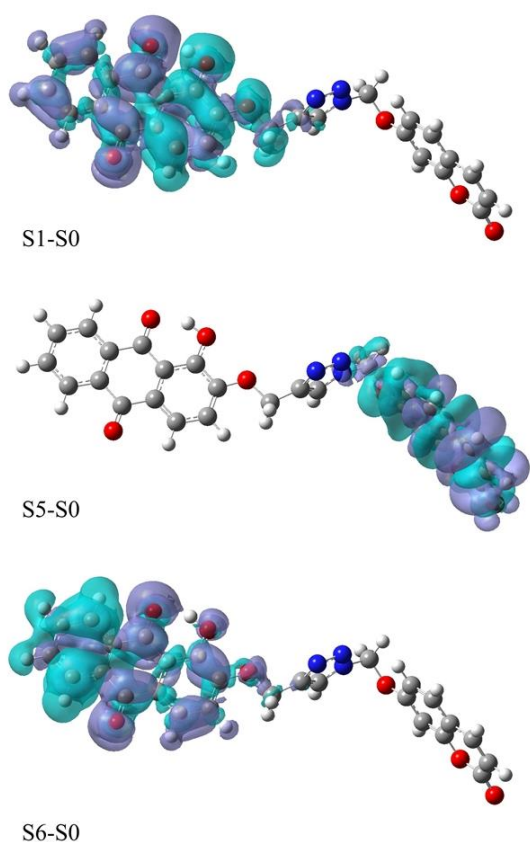


Fig. 6

3D plots of the electron density difference between the ground S_0 and the first S_1 (top), the fifth S_5 (centre) and sixth S_6 (bottom) electronic state computed for the 5C conformer. The zones where the electron density

As expected in view of the substantial decoupling of the two chromophores and in agreement with the experimental observations, the sum of *Dn* and *Ac* individual spectra well reproduces the computed

Bi spectra. Our calculations semi-quantitatively reproduce the slight hypsochromic shift on the lowest energy band of the **Bi** with respect to the **Ac+Dn** sum observed in the experiment. This band centred at 400 nm is due to the HOMO \rightarrow LUMO transition to the first excited state of **Bi**. The VE of this excitation is 373 nm, a value close to the 376 nm of the VE of the HOMO \rightarrow LUMO transition to the first excited state of **Ac**.

The frontier molecular orbitals of **Bi** are shown in Fig. 6, taking the most stable 5C conformation as an example; the complete localization on the **Ac** and **Dn** moieties is evident. We notice first that, as shown in Fig. 5, the HOMO and LUMO of **Bi** are very similar to those of **Ac**, shown in Fig.S3 (see Supplementary Information). The 3D map of the electron density difference between the first excited and the ground electronic states (S1-S0), see Fig.6, shows that this transition is localized on **Ac**, thus implying the absence of electron transfer between the two chromophores during the excitation. The **Bi** absorption band centered at 300 nm results from the sum of two different excitations: to the fifth (S5) and to the sixth (S6) excited states. The first is the less intense and it is essentially due to the HOMO-4 \rightarrow LUMO transition. It is characterized by a VE of 290 nm, very close to the transition to the second excited state of **Ac** (289 nm). The localization of this transition on **Ac** is also confirmed by the MO analysis and by the electron density difference map, shown in Fig.S3 (see Supplementary Information). The excitation to S6 is more intense and it is due to the HOMO-1 \rightarrow LUMO+1 transition. The shape of the latter is in very good agreement with HOMO and LUMO of **Dn**. Also in this case, the VE excitation is 286 nm, very close to the VE transition to the first excited state of **Dn**, i.e. 289 nm.

All the presented results show that there is no electron density exchange between **Dn** and **Ac** upon the analysed excitations. This implies that the two molecular units, although connected by a triazole bridge, behave as isolated chromophores. The bridge has only a structural function, and does not modify the spectroscopic properties of monomer units. The insulating character of the triazole ring was also confirmed in a recent publication by D. Bai et al.⁹⁷ The MOs involved in the absorption and emission of **Bi** are localized on the two distinct chromophores, and do not present significant differences with respect to the orbitals involved in the electronic transitions of the isolated **Dn** and **Ac**. The behaviours of all the configurations of **Bi** are very similar, including that of AAC (see Supplementary Information, Figs. S7 and S8), and the change of the relative positions of **Dn** and **Ac** does not affect the absorption and emission spectra.

Discussion

The experimental data reported above highlight a very fast and efficient intramolecular electronic energy transfer process. In order to understand the reasons determining these experimental

observations it is important to model the mechanism responsible of the intra-EET; in other words, to clarify how **Dn** and **Ac** interact. A recurring important problem in resonance energy transfer is the ability to discriminate between strong, intermediate and weak regimes for the electronic coupling. Förster theory was formulated within the weak coupling limit; in fact, it is based on the application of the equilibrium Fermi Golden-rule, with second-order perturbation theory treatment of electronic coupling between donor and acceptor. Two are the fundamental assumption of the Förster model: a) following the electronic excitation of the donor, the bath equilibrates on a time scale faster than EET, b) the coupling with the bath is stronger than the coupling between donor and acceptor.

The inhomogeneously broadened absorption spectra, Fig.1, demonstrate that **Dn** and **Ac** are strongly coupled with the solvent, while the very small difference between the bichromophore's spectrum and the sum of the spectra **Dn+Ac** is indicative of the weak intramolecular interaction between the two moieties. Confirmation of these evidences comes from the calculated electron densities difference for the excited state of **Bi** (Fig. 6) from which results clear the absence of electron density on the triazole ring for the S1-S0, S5-S0 and the S6-S0 transitions. Hence, the *weak*-coupling regime can be considered as a good approximation for the energy transfer process in **Bi**. In the weak coupling regime when the donor-acceptor distance is greater than the sum of the Van der Waals radii, the electronic coupling can be primarily described by the Coulomb interaction between **Dn** and **Ac**. Approximating the Coulomb coupling as the interaction between transition dipole moments of donor and acceptor molecules, the transfer rate constant is calculated from experimental data using the Förster relation:^{1,}

20, 21

$$k^F = \frac{9000 \ln(10) k^2 \Phi_D}{128 \pi^5 n^4 N \tau_D R^6} J(\tilde{\nu}) \quad (7)$$

$$J(\tilde{\nu}) = \int_0^\infty \frac{f_D(\tilde{\nu}) \alpha_A(\tilde{\nu})}{\tilde{\nu}^4} d\tilde{\nu}$$

In this expression k is the orientation factor associated with the dipole-dipole interaction between donor and acceptor, R is their centre-to-centre separation in units of cm, n is the refractive index of the medium, N is Avogadro's number, Φ_D is the donor fluorescence quantum yield, and τ_D is the lifetime of the donor. The Förster spectral overlap $J(\tilde{\nu})$, given in units of $M^{-1}cm^3$, can be calculated from the experimental data as the overlap, on a wavenumber scale, of the absorption spectrum of the acceptor $\alpha_A(\tilde{\nu})$, where the intensity is in molar absorbance, with the area-normalized emission spectrum of the donor, $f_D(\tilde{\nu})$. Because we directly measured the *EET* rate constant ($\tau \sim 1.5$ ps) using transient absorption spectroscopy, we can calculate the **Dn-Ac** distance compatible with the measured *EET* time constant $\tau \sim 1.5$ ps, and compare the result obtained with the prediction of the DFT conformational analysis. If we assume as a first approximation that the orientation factor is equal to

2/3 (random mutual orientation between **Dn** and **Ac**) we obtain a distance of ~ 11 Å. Conformational analysis revealed the presence of eleven main conformations of **Bi**. They are schematically reported in Table 2, together with the population percentages. Using the statistical weights from Table 2 and the distances between the two chromophores, shown in Table 3, we obtain an average distance of ~ 12 Å between **Dn** and **Ac** in **Bi**, a value in very good agreement with the one estimated from Förster equation.

Table 3: Full *ab initio* transfer time constants and dipole-dipole coupling for the energy transfer from **Dn** to **Ac** for different conformations of **Bi**. $n^2 = 1.80$ for all conformations except for AAC, where $n^2 = 1$.

Conformer	R [Å]	$I(\tilde{\nu}) \cdot 10^{15}$ [s]	κ^2	$ \mu_D $ [au]	$ \mu_A $ [au]	I/k^F [ps]
5C	13.500	3.00	3.180	2.333	1.945	3.0
6C	13.411	2.88	3.111	2.329	1.943	3.0
7C	10.747	3.02	1.579	2.287	1.889	1.7
8C	12.878	3.06	1.684	2.110	1.932	5.1
9C	12.921	3.11	1.678	2.114	1.934	5.1
10C	10.561	3.00	0.849	2.098	1.892	3.3
12C	10.472	3.04	0.837	2.096	1.891	3.2
AAC	7.523	2.88	1.073	2.231	1.720	0.2

One of the aims of this work is to verify if the dipole-dipole coupling is actually a good approximation for the electronic coupling between **Dn** and **Ac**, given the high efficiency and fast rate of energy transfer observed in this bichromophoric system. Furthermore, we want to investigate whether there are preferential conformations for EET and, in that case, to understand if any preference arises from geometrical, electronic or vibronic factors. A number of assumptions are necessary to perform the computation of the rate constant. First, the Coulomb electronic coupling V^{Coul} is approximated as a dipole-dipole interaction V^{dd} :

$$V = V^{Coul} \approx V^{dd} = \frac{1}{4n^2 \pi \epsilon_0} \frac{k \mu_D \mu_A}{R^3} \quad (8)$$

The *EET* rate constant is then calculated as:

$$k^F = \frac{2\pi}{\hbar} |V^{dd}|^2 I(\tilde{\nu}) \quad (9)$$

where $I(\tilde{\nu})$ is the overlap integral between absorption ($N_A a_A(\tilde{\nu}) \tilde{\nu}^{-1}$) and emission ($N_D f_D(\tilde{\nu}) \tilde{\nu}^{-3}$) lineshapes, and N_A and N_D are normalization factors (i.e. the areas are normalized to 1). This quantity reflects the contribution of the Franck-Condon factors to the EET rate and is strictly related to the

experimental J in Eq. 7, but, at variance with the latter, it does not include the effect of the transition dipoles since they are explicitly accounted for in the coupling in Eq. 8. For the pertinent states of **Bi** we adopted in our calculation FC|VG Gaussian lineshapes with HWHM = 800 cm⁻¹. As discussed in previous sections, this value is very close to the ab initio prediction for the solvent inhomogeneous broadening for **Dn**, while it is 30% too small for **Ac**, possibly causing a slight underestimation of J (and of the rate constant). R was calculated as the distance of the centre of mass of **Ac** and **Dn** in **Bi**. For the square of the refractive index n^2 of acetonitrile we used the value 1.80 for all conformations, except for the AAC conformation. In fact, from the analysis of the shape of the PCM cavity of this conformation (see Figure S5), the volume between the two chromophores is hardly accessible to the solvent, differently from what happens in the other structures. Therefore, in AAC case n^2 was set equal to 1. Moreover, in the calculation of the orientation factor k , the transition dipole moments of the individual chromophores were identified with the transition dipole moments of **Bi**. More precisely, taking into account the analysis of the simulated absorption and emission spectra, the transition dipole moment of S0-S1 transition was attributed to **Ac** and the transition dipole of S0-S6 transition to **Dn**. While these assumptions surely have an effect on the predicted value of the transfer rate k^F , we believe that the application of such computational protocol allows to semi-quantitatively investigate the relative differences of the EET rates of the various conformers, which in turn arises from a balance of several factors. A dominant role is played by the intermolecular distance between **Ac** and **Dn** that varies between 10.5 and 13.5 Å in the most stable conformations; only for AAC we obtain a substantially smaller value (7.5 Å). A second factor that significantly modulates the EET rate is the relative orientation of the transition dipoles of **Ac** and **Dn**: it produces for the different conformations a variation of k^2 from ~0.8 to ~3.2. The 5C and 6C conformations exhibit the largest k^2 , i.e. 3.180 and 3.111, due to the nearly parallel arrangement of **Ac** and **Dn**, while the 10C and 12C conformations have the smallest ones, i.e. 0.849 and 0.837, because here **Ac** and **Dn** are quite close to a perpendicular arrangement. The differences in the transition dipoles' lengths modulate only slightly the EET rate (within 15%). Finally, the $I(\tilde{\nu})$ integral, i.e. the vibronic contribution to the energy transfer process appears very similar in all the conformers and differentiate only slightly their EET rate (6 %). In this respect we should highlight that the position and the shape of the FC|VG spectra cannot be considered totally accurate. The computed emission (**Dn**) and absorption (**Ac**) spectra are slightly more separated than the experimental ones (~400 cm⁻¹ as far as the distance between the maxima is considered). Correcting for this error we roughly have a 10% increase of the EET rate. It is noteworthy that due to the low-resolution of the spectra, one of the most relevant effects expected by the introduction of Duschinsky mixings and frequency changes (neglected in the VG level) is a shift of the zero-point-energies and a consequent shift of the whole spectrum⁹⁸. For the

deprotonated form of alizarin this shift is $\sim 650 \text{ cm}^{-1}$,⁹⁹ while for umbelliferone it is $\sim 800 \text{ cm}^{-1}$, leading to the relative shift of about 150 cm^{-1} , in line with the discrepancy between simulated and experimental spectra of the bichromophore. The AAC conformation deserves some special comment. Its Boltzmann population is small but this conformer is not completely negligible since its sensibly shorter inter-chromophore distance leads to a rate constant an order of magnitude larger than that for the other conformations. It should be highlighted however that for such a short distance the approximated expression for the coupling in Eq.8 is probably not adequate.

Taking into account the relative population abundance of the different conformations and their EET rate constants one obtains a decay profile that is nicely fitted with a mono-exponential with a time constant $\sim 3.5 \text{ ps}$ (see supporting info for details); the weighted average of the EET time constants of Table 3 is $\sim 3.6 \text{ ps}$. This fully ab initio value is in reasonable agreement with the experimental observation $\tau_{EET} = 1.5 \pm 0.5 \text{ ps}$. The difference is not surprising due to the number of approximation in our treatment and can be due to inaccuracy in the relative stabilities of the conformers and in the calculations of the factors that determine their EET rates. More specifically, the fact that the predicted EET rate is slower than the experimental one suggests that either our calculations underestimate the abundance of the AAC conformer, or the dipole approximation underestimates the coupling between **Dn** and **Ac**. On this respect it should be noticed that, according to Förster theory, in Eq. 8 we assumed that the screening factor for the coupling of the two dipoles is $s=1/n^2$. In ref. 100 Caprasecca *et al.* modelled this effect more accurately within polarizable continuum model, and they showed that for a system with an interchromophoric distance similar to that of **Bi**, the Onsager expression $s = 3(2n^2 + 1)^{-1}$ is more accurate than $s = 1/n^2$. If we adopt the Onsager model for **Bi** we obtain an enhancement of the coupling by $\sim 20 \%$, corresponding to an estimated EET rate $\sim 2.56 \text{ ps}$, in better agreement with experiment. As a last comment, we notice that the fact that the multi-exponential theoretical decay is well reproduced by a phenomenological mono-exponential function explains why a single decay constant is observed experimentally, despite the fact that a number of conformations contribute to the process with different rate constants.

Conclusions

In this work we presented the synthesis and the spectroscopic and computational characterization of the bichromophore (**Bi**) composed by the donor-acceptor couple Umbelliferone-Alizarin. We verified the presence of energy transfer between **Dn** and **Ac** from the quenching of the fluorescence of **Dn** in the presence of **Ac** ($\Phi_{Dn} = 0.011$, $\Phi'_{Dn} = 0.0016$). The calculated transfer efficiency resulted 85%. We performed transient absorption measurements and DFT quantum chemical calculations to shed light on the mechanism that underlies the *EET* in this bichromophore. The time-resolved experiments

reveal a very fast transfer process, with a time constant, obtained with the fitting model described in eqs. 2 and eq. 3, of 1.5 ± 0.5 ps. The very weak coupling between **Dn** and **Ac**, with respect to the coupling that **Dn** and **Ac** have with the surrounding bath, is clearly demonstrated by the homogeneously broadened absorption spectrum line-shape of **Bi** (Fig.1) and by the close correspondence of the spectrum of **Bi** with the sum of the absorption spectra of isolated **Dn** and **Ac**. The calculation of the electronic structure of **Bi** pointed out that the through-bond interactions between the electron densities of **Dn** and **Ac** is practically absent (Fig. 5 and Fig. 6). Both the experimental and computational results indicate that *EET* in **Bi** is fully compatible with the *weak-coupling* regime between **Dn** and **Ac**. We used the Förster relation (eq. 7) to calculate the average distance between **Dn** and **Ac**, obtaining a value of ~ 11 Å. To validate this approach we performed a conformational analysis at DTF level on **Bi** in order to extract the most representative conformers. Then we calculated the average distance between the centre of mass of **Dn** and **Ac** in **Bi** obtaining a value of ~ 12 Å. The very good agreement of the distance calculated using the Förster equation with the one obtained from the conformational analysis makes us very confident that the dipole-dipole approximation for the Coulombic coupling between **Dn** and **Ac** is a good model to describe the *EET* in **Bi**. In the final part of the work, making use of eq. 8 and eq. 9 we calculated the transfer rate constants for the various conformers adopting a fully *ab-initio* approach. We can conclude that the weak-coupling regime and the dipole-dipole interaction is still a good model for the description of the energy transfer in molecular systems where the distance between **Dn** and **Ac** is comparable with the sizes of the donor and of the acceptor moieties, provided that the through bond interactions are sufficiently weak.

Acknowledgments

The authors acknowledge the financial support of the Italian MIUR (FIRB ‘Futuro in Ricerca’ 2010, RBFR10Y5VW to M.D.D. and C.C.; FIRB ‘Futuro in Ricerca’ 2010, RBFR109ZHQ to A.L.; PRIN 2010-2011 “Frontiers studies in molecular spectroscopy and dynamics” to F. S. and R. R.). The financial support of the Cassa di Risparmio di Firenze is also gratefully acknowledged. C.C. acknowledges support from COST (Action CODECS: CONvergent Distributed Environment for Computational Spectroscopy). A.L. acknowledges the support of Regione Toscana through PORFSE 2007-2013, project EPHODS.

References

1. A. Olaya-Castro and G. D. Scholes, *International Reviews in Physical Chemistry*, 2011, **30**, 49-77.
2. G. D. Scholes, G. R. Fleming, A. Olaya-Castro and R. van Grondelle, *Nat Chem*, 2011, **3**, 763-774.
3. M. R. Shortreed, S. F. Swallen, Z.-Y. Shi, W. Tan, Z. Xu, C. Devadoss, J. S. Moore and R. Kopelman, *The Journal of Physical Chemistry B*, 1997, **101**, 6318-6322.
4. A. Adronov and J. M. J. Frechet, *Chemical Communications*, 2000, 1701-1710.
5. V. S. F. Balzani, *Supramolecular Photochemistry (Ellis Horwood Series in Physical Chemistry)*, Ellis Horwood Ltd, 1991.
6. D. Gust, T. A. Moore and A. L. Moore, *Accounts of Chemical Research*, 2001, **34**, 40-48.
7. I. L. Medintz and H. Mattoussi, *Physical Chemistry Chemical Physics*, 2009, **11**, 17-45.
8. H. van Amerongen and R. van Grondelle, *The Journal of Physical Chemistry B*, 2000, **105**, 604-617.
9. H. v. Amerongen, R. v. Grondelle and L. Valkunas, *Photosynthetic Excitons*, World Scientific Publishers, 2000.
10. W. G. J. H. M. v. Sark, K. W. J. Barnham, L. H. Slooff, A. J. Chatten, A. Büchtemann, A. Meyer, S. J. McCormack, R. Koole, D. J. Farrell, R. Bose, E. E. Bende, A. R. Burgers, T. Budel, J. Quilitz, M. Kennedy, T. Meyer, C. D. M. Donegá, A. Meijerink and D. Vanmaekelbergh, *Opt. Express*, 2008, **16**, 21773-21792.
11. P. F. Scudo, L. Abbondanza, R. Fusco and L. Caccianotti, *Solar Energy Materials and Solar Cells*, 2010, **94**, 1241-1246.
12. A. Mirloup, P. Retailleau and R. Ziessel, *Tetrahedron Letters*, 2013, **54**, 4456-4462.
13. E. K. L. Yeow, D. J. Haines, K. P. Ghiggino and M. N. Paddon-Row, *The Journal of Physical Chemistry A*, 1999, **103**, 6517-6524.
14. D. Gust, T. A. Moore and A. L. Moore, *Accounts of Chemical Research*, 2009, **42**, 1890-1898.
15. I. McConnell, G. Li and G. W. Brudvig, *Chemistry & biology*, 2010, **17**, 434-447.
16. V. Balzani, A. Credi and M. Venturi, *ChemSusChem*, 2008, **1**, 26-58.
17. C. Smyth, F. Fassiooli and G. D. Scholes, *Philosophical Transactions of the Royal Society A: Mathematical, Physical and Engineering Sciences*, 2012, **370**, 3728-3749.
18. J. M. Anna, Y. Song, R. Dinshaw and G. D. Scholes, *Pure and Applied Chemistry*, 2013, **85**, 1307-1319.
19. S. Speiser, *Chemical Reviews*, 1996, **96**, 1953-1976.
20. G. D. Scholes, *Annual Review of Physical Chemistry*, 2003, **54**, 57-87.
21. T. Förster, *Annalen der Physik*, 1948, **437**, 55-75.
22. P. G. Wu and L. Brand, *Analytical Biochemistry*, 1994, **218**, 1-13.
23. W. E. Wymann, R. Davis, J. W. Patterson and J. R. Pfister, *Synthetic Communications*, 1988, **18**, 1379-1384.
24. M. R. Dhananjeyan, Y. P. Milev, M. A. Kron and M. G. Nair, *Journal of Medicinal Chemistry*, 2005, **48**, 2822-2830.
25. H. Singh and R. Warmuth, *Tetrahedron*, 2002, **58**, 1257-1264.
26. Y.-C. Duan, Y.-C. Ma, E. Zhang, X.-J. Shi, M.-M. Wang, X.-W. Ye and H.-M. Liu, *European Journal of Medicinal Chemistry*, 2013, **62**, 11-19.
27. S. Cicchi, P. Fabbrizzi, G. Ghini, A. Brandi, P. Foggi, A. Marcelli, R. Righini and C. Botta, *Chemistry – A European Journal*, 2009, **15**, 754-764.
28. A. M. Brouwer, *Pure and Applied Chemistry*, 2011, **83**, 2213-2228.
29. A. Feis, A. Lapini, B. Catacchio, S. Brogioni, P. Foggi, E. Chiancone, A. Boffi and G. Smulevich, *Biochemistry*, 2008, **47**, 902-910.
30. P. Tournon Touceda, S. Mosquera Vazquez, M. Lima, A. Lapini, P. Foggi, A. Dei and R. Righini, *Physical Chemistry Chemical Physics*, 2012, **14**, 1038-1047.
31. A. Lapini, P. Foggi, L. Bussotti, R. Righini and A. Dei, *Inorganica Chimica Acta*, 2008, **361**, 3937-3943.
32. A. Marcelli, P. Foggi, L. Moroni, C. Gellini and P. R. Salvi, *The Journal of Physical Chemistry A*, 2008, **112**, 1864-1872.
33. M. J. Frisch, G. W. Trucks, H. B. Schlegel, G. E. Scuseria, M. A. Robb, J. R. Cheeseman, J. A. Montgomery, J. T. Vreven, K. N. Kudin, J. C. Burant, J. M. Millam, S. S. Iyengar, J. Tomasi, V. Barone, B. Mennucci, M. Cossi, G. Scalmani, N. Rega, G. A. Petersson, H. Nakatsuji, M. Hada, M. Ehara, K. Toyota, R. Fukuda, J. Hasegawa, M. Ishida, T. Nakajima, Y. Honda, O. Kitao, H. Nakai, M.

- Klene, X. Li, J. E. Knox, H. P. Hratchian, J. B. Cross, C. Adamo, J. Jaramillo, R. Gomperts, R. E. Stratmann, O. Yazyev, A. J. Austin, R. Cammi, C. Pomelli, J. W. Ochterski, P. Y. Ayala, K. Morokuma, G. A. Voth, P. Salvador, J. J. Dannenberg, V. G. Zakrzewski, S. Dapprich, A. D. Daniels, M. C. Strain, O. Farkas, D. K. Malick, A. D. Rabuck, K. Raghavachari, J. B. Foresman, J. V. Ortiz, Q. Cui, A. G. Baboul, S. Clifford, J. Cioslowski, B. B. Stefanov, G. Liu, A. Liashenko, P. Piskorz, I. Komaromi, R. L. Martin, D. J. Fox, T. Keith, M. A. Al-Laham, C. Y. Peng, A. Nanayakkara, M. Challacombe, P. M. W. Gill, B. Johnson, W. Chen, M. W. Wong, C. Gonzalez and J. A. Pople, *Gaussian development version H21*, (2009) Gaussian, Inc., Wallingford CT.
34. A. D. Becke, *Journal of Chemical Physics*, 1993, **98**, 5648.
 35. P. J. Stephens, F. J. Devlin, C. F. Chabalowski and M. J. Frisch, *The Journal of Physical Chemistry*, 1994, **98**, 11623-11627.
 36. C. Lee, W. Yang and R. G. Parr, *Phys. Rev. B*, 1988, **37**, 785-789.
 37. T. Yanai, D. P. Tew and N. C. Handy, *Chemical Physics Letters*, 2004, **393**, 51-57.
 38. *Basis sets of the N07 and SNS families are available for download: <http://dreams.sns.it> (Accessed April 2013).*
 39. V. Barone, P. Cimino and E. Stendardo, *Journal of Chemical Theory and Computation*, 2008, **4**, 751-764.
 40. C. Puzzarini, M. Biczysko and V. Barone, *Journal of Chemical Theory and Computation*, 2010, **6**, 828-838.
 41. V. Barone, J. Bloino and M. Biczysko, *Physical Chemistry Chemical Physics*, 2010, **12**, 1092-1101.
 42. V. Barone and M. Cossi, *The Journal of Physical Chemistry A*, 1998, **102**, 1995-2001.
 43. M. Cossi, N. Rega, G. Scalmani and V. Barone, *Journal of Computational Chemistry*, 2003, **24**, 669-681.
 44. J. Tomasi, B. Mennucci and R. Cammi, *Chem. Rev.*, 2005, **105**, 2999.
 45. F. Floris and J. Tomasi, *Journal of Computational Chemistry*, 1989, **10**, 616-627.
 46. F. M. Floris, J. Tomasi and J. L. P. Ahuir, *Journal of Computational Chemistry*, 1991, **12**, 784-791.
 47. R. A. Pierotti, *Chemical Reviews*, 1976, **76**, 717-726.
 48. F. Furche and R. Ahlrichs, *The Journal of Chemical Physics*, 2002, **117**, 7433-7447.
 49. G. Scalmani, M. J. Frisch, B. Mennucci, J. Tomasi, R. Cammi and V. Barone, *The Journal of Chemical Physics*, 2006, **124**, 094107-094115.
 50. M. Cossi and V. Barone, *The Journal of Chemical Physics*, 2001, **115**, 4708-4717.
 51. R. Cammi, S. Corni, B. Mennucci and J. Tomasi, *The Journal of Chemical Physics*, 2005, **122**, 104513-104512.
 52. S. Corni, R. Cammi, B. Mennucci and J. Tomasi, *The Journal of Chemical Physics*, 2005, **123**, 134512-134510.
 53. A. V. Marenich, C. J. Cramer, D. G. Truhlar, C. A. Guido, B. Mennucci, G. Scalmani and M. J. Frisch, *Chemical Science*, 2011, **2**, 2143-2161.
 54. F. Santoro, R. Improta, A. Lami, J. Bloino and V. Barone, *The Journal of Chemical Physics*, 2007, **126**, 084509-084513.
 55. V. Barone, J. Bloino, M. Biczysko and F. Santoro, *Journal of Chemical Theory and Computation*, 2009, **5**, 540-554.
 56. J. Bloino, M. Biczysko, F. Santoro and V. Barone, *Journal of Chemical Theory and Computation*, 2010, **6**, 1256-1274.
 57. V. Barone, A. Baiardi, M. Biczysko, J. Bloino, C. Cappelli and F. Lipparini, *Physical Chemistry Chemical Physics*, 2012, **14**, 12404-12422.
 58. J. B. M. Biczysko, F. Santoro and V. Barone, in *Computational Strategies for Spectroscopy: from Small Molecules to Nano Systems*, ed. V. Barone, John Wiley & Sons, Inc, 2011, pp. 361-443.
 59. F. J. Avila Ferrer and F. Santoro, *Physical Chemistry Chemical Physics*, 2012, **14**, 13549-13563.
 60. J. Franck and E. G. Dymond, *Transactions of the Faraday Society*, 1926, **21**, 536-542.
 61. E. U. Condon, *Physical Review*, 1928, **32**, 858-872.
 62. F. J. A. Ferrer, R. Improta, F. Santoro and V. Barone, *Physical Chemistry Chemical Physics*, 2011, **13**, 17007-17012.
 63. D. W. Fink and W. R. Koehler, *Anal. Chem.*, 1970, **42**, 990.
 64. G. J. Yakatan, R. J. Juneau and S. G. Schulman, *Anal. Chem.*, 1972, **44**, 1044.
 65. E. Bardez, P. Boutin and B. Valeur, *Chemical Physics Letters*, 1992, **191**, 142.

66. M. Hoshiyama, K. Kubo, T. Igarashi and T. Sakurai, *Journal of Photochemistry and Photobiology A: Chemistry*, 2001, **138**, 227 - 233.
67. N. Nizomov, A. U. Kholov, A. A. Ishchenko, V. V. Ishchenko and V. P. Khilya, *Journal of Applied Spectroscopy*, 2007, **74**, 626.
68. J. R. Heldt, J. Heldt, M. Stofi and H. A. Diehl, *Spectrochimica Acta Part A*, 1995, **51**, 1549.
69. J. S. de Melo and P. F. Fernandes, *J. mol. struct.*, 2001, **565-566**, 69.
70. J. S. de Melo and A. L. Macanita, *Chemical Physics Letters*, 1993, **204**, 556.
71. G. Smulevich and P. Foggi, *The Journal of Chemical Physics*, 1987, **87**, 5657-5663.
72. G. Smulevich, P. Foggi, A. Feis and M. P. Marzocchi, *The Journal of Chemical Physics*, 1987, **87**, 5664-5669.
73. A. Weller, *Prog. React. Kinet.*, 1961, **1**, 187.
74. A. Weller, *Z. Elektrochem*, 1956, **60**, 1144.
75. C. Miliani, A. Romani and G. Favaro, *Spectrochimica Acta Part A*, 1998, **54**, 581 - 588.
76. R. A. Bhat, in *Laboratory Techniques in Biochemistry and Molecular Biology*, ed. T. W. J. Gadella, Elsevier, 2009, vol. Volume 33, pp. 413-445.
77. A. Lapini, S. Mosquera Vázquez, P. Tourón Touceda and M. Lima, *Journal of Molecular Structure*, 2011, **993**, 470-473.
78. K. Ekvall, P. van der Meulen, C. Dhollande, L.-E. Berg, S. Pommeret, R. Naskrecki and J.-C. Mialocq, *Journal of Applied Physics*, 2000, **87**, 2340-2352.
79. M. Lorenc, M. Ziolk, R. Naskrecki, J. Karolczak, J. Kubicki and A. Maciejewski, *Appl. Phys. B*, 2002, **74**, 19.
80. P.-T. Chou, M. L. Martinez and S. L. Studer, *Chemical Physics Letters*, 1992, **188**, 49.
81. P. Foggi, L. Pettini, I. Santa, R. Righini and S. Califano, *The Journal of Physical Chemistry*, 1995, **99**, 7439-7445.
82. D. A. V. Kliner, J. C. Alfano and P. F. Barbara, *The Journal of Chemical Physics*, 1993, **98**, 5375-5389.
83. S. A. Kovalenko, R. Schanz, H. Hennig and N. P. Ernsting, *The Journal of Chemical Physics*, 2001, **115**, 3256-3273.
84. K.-L. Han and G.-J. Zhao, *Hydrogen Bonding and Transfer in the Excited State*, John Wiley & Sons Lt, 2011.
85. S. Y. Arzhantsev, S. Takeuchi and T. Tahara, *Chemical Physics Letters*, 2000, **330**, 83-90.
86. P.-T. Chou, Y.-C. Chen, W.-S. Yu and Y.-M. Cheng, *Chemical Physics Letters*, 2001, **340**, 89-97.
87. J. R. Choi, S. C. Jeoung and D. W. Cho, *Chemical Physics Letters*, 2004, **385**, 384-388.
88. D. W. Cho, S. H. Kim, M. Yoon and S. C. Jeoung, *Chemical Physics Letters*, 2004, **391**, 314-320.
89. F. V. R. Neuwahl, L. Bussotti, R. Righini and G. Buntinx, *Physical Chemistry Chemical Physics*, 2001, **3**, 1277-1283.
90. M. A. R. Matos, C. C. S. Sousa, M. S. Miranda, V. M. F. Morais and J. F. Liebman, *The Journal of Physical Chemistry B*, 2009, **113**, 11216-11221.
91. G.-Y. Li, G.-J. Zhao, K.-L. Han and G.-Z. He, *Journal of Computational Chemistry*, 2011, **32**, 668-674.
92. C. C. S. Sousa, M. A. R. Matos and V. M. F. Morais, *The Journal of Chemical Thermodynamics*, 2011, **43**, 1435-1440.
93. S. H. Cho, H. Huh, H. M. Kim, C. I. Kim, N. J. Kim and S. K. Kim, *J. Chem. Phys.*, 2005, **122**, 34304.
94. R. Improta, V. Barone, G. Scalmani and M. J. Frisch, *The Journal of Chemical Physics*, 2006, **125**, 054103-054109.
95. R. Improta, G. Scalmani, M. J. Frisch and V. Barone, *The Journal of Chemical Physics*, 2007, **127**, 074504-074509.
96. M. J. Frisch, G. W. Trucks, H. B. Schlegel, G. E. Scuseria, M. A. Robb, J. R. Cheeseman, J. A. Montgomery, J. T. Vreven, K. N. Kudin, J. C. Burant, J. M. Millam, S. S. Iyengar, J. Tomasi, V. Barone, B. Mennucci, M. Cossi, G. Scalmani, N. Rega, G. A. Petersson, H. Nakatsuji, M. Hada, M. Ehara, K. Toyota, R. Fukuda, J. Hasegawa, M. Ishida, T. Nakajima, Y. Honda, O. Kitao, H. Nakai, M. Klene, X. Li, J. E. Knox, H. P. Hratchian, J. B. Cross, C. Adamo, J. Jaramillo, R. Gomperts, R. E. Stratmann, O. Yazyev, A. J. Austin, R. Cammi, C. Pomelli, J. W. Ochterski, P. Y. Ayala, K. Morokuma, G. A. Voth, P. Salvador, J. J. Dannenberg, V. G. Zakrzewski, S. Dapprich, A. D. Daniels, M. C. Strain, O. Farkas, D. K. Malick, A. D. Rabuck, K. Raghavachari, J. B. Foresman, J. V. Ortiz,

- Q. Cui, A. G. Baboul, S. Clifford, J. Cioslowski, B. B. Stefanov, G. Liu, A. Liashenko, P. Piskorz, I. Komaromi, R. L. Martin, D. J. Fox, T. Keith, M. A. Al-Laham, C. Y. Peng, A. Nanayakkara, M. Challacombe, P. M. W. Gill, B. Johnson, W. Chen, M. W. Wong, C. Gonzalez and J. A. Pople, *Revision D.01*, (2013) Gaussian, Inc., Wallingford CT.
97. D. Bai, A. C. Benniston, J. Hagon, H. Lemmetyinen, N. V. Tkachenko and R. W. Harrington, *Physical Chemistry Chemical Physics*, 2013, **15**, 9854-9861.
98. F. J. Avila Ferrer, J. Cerezo, E. Stendardo, R. Improta and F. Santoro, *Journal of Chemical Theory and Computation*, 2013, **9**, 2072-2082.
99. L. Carta, M. Biczysko, J. Bloino, D. Licari and V. Barone, *Physical Chemistry Chemical Physics*, 2013.
100. S. Caprasecca, C. Curutchet, B. Mennucci, *Photochemical & Photobiological Sciences* 2011, **10**, 1602-9